Energy 290 (2024) 130315

Contents lists available at ScienceDirect

Energy

journal homepage: www.elsevier.com/locate/energy

Operation and control of compact offshore combined cycles for power generation

Rubén M. Montañés, Cristina Zotică, Adriana Reyes-Lúa *

SINTEF Energy Research, Sem Sælandsvei 11, Trondheim, 7034, Norway

ARTICLE INFO

Keywords:
Combined cycle
Once-through steam-generator
Steam bottoming cycle
Decentralized control
Nonlinear feedforward
Efficiency
CO_2 intensity

ABSTRACT

Gas turbines are the main means for generating power in offshore installations. To increase energy efficiency, and thus reduce CO_2 emissions, a steam bottoming cycle can be added to produce additional power by recovering surplus heat from the gas turbine exhaust. Due to space constraints, this solution is not widespread for offshore power generation. To enable deployment, the system must be compact and be able to provide varying power demands. In this paper, we analyze the operation and control problem for such *compact* combined cycles, consisting of two gas turbines and one steam bottoming cycle. We analyze the steady-state performance of the combined cycle with respect to efficiency and CO_2 emissions for two control strategies for coordinating the power setpoint of the two gas turbines. Equal load allocation of the gas turbines showed a higher thermal efficiency and lower emissions compared to keeping one gas turbine close to nominal and letting the second one handle load variations. The main controlled variables for the steam bottoming cycle are the superheated steam pressure and temperature. We implement decentralized control strategies based on standard PID-controllers and nonlinear feedforward. Due to reduced throttle losses, sliding pressure shows higher efficiency and lower CO_2 emissions compared to keeping a constant steam pressure, which conversely provides a better temperature dynamic response and may be necessary with highly varying power demand.

1. Introduction

Gas turbines are the main source for generating electric and mechanical power, as well as heat, in offshore oil and gas installations. Offshore gas turbines use readily available natural gas as fuel, and they are the largest greenhouse gas (GHG) emission source for offshore oil and gas activities. For example, in 2020 gas turbines had a share of 85% of the $CO_{2,eq}$ emissions on the Norwegian Continental Shelf (NCS), where there is a long history of measures to reduce emissions from offshore activities, to some extent due to a carbon tax, which is levied on all combustion of gas, oil and diesel in petroleum operations on the NCS and on releases of CO_2 and natural gas. Despite recent efforts to further reduce the emissions from gas turbines, such as supplying power with low CO_2 footprint from shore or from floating offshore wind farms, in 2022 gas turbines still accounted for 80.73% of the $CO_{2,eq}$ emissions in the NCS [1]. This is in part because gas turbines offer several operational and design advantages compared to other potential power generation technologies. Among others, high power to weight ratio and the capability of changing the load fast to balance supply and demand of electric power, which is a requirement in offshore power generation systems, as they are typically not connected to a grid and operate in island mode [2].

In most offshore installations, gas turbines operate in an open cycle configuration, i.e., simple gas turbines, with a design thermal (LHV) efficiency of ~35%–40% [3,4]. Thermal efficiencies are highest at full-load and are reduced at part-load operation. Despite this, most offshore units operate part-load in a load-share scheme to assure reliability and stability in the island power system [5].

If there is heat demand in the topside operations, e.g., for oil and gas separation, the heat in the gas turbine exhaust gas is recovered using a waste heat recovery unit (WHRU). The potential to make use of this heat strongly depends on the process heat demand of the specific site [2,3,6]. The heat in the gas turbine exhaust gas can also be used to produce steam in a heat recovery steam generator (HRSG). This steam can drive a steam turbine, producing additional electricity in a steam bottoming cycle. The bottoming cycle increases the thermal efficiency with respect to an open cycle, with a combined cycle (CCGT) efficiency of ~45-50% [2–4,7]. Moreover, the bottoming cycle dampens the decrease in efficiency for part-load operation [8,9]. With an increased efficiency, the consumption of fuel gas and the emissions of CO_2 and NO_x are decreased by ~25% with combined cycles [2–4]. Additional total emission reductions can be achieved if the number of gas turbines operating in an installation is reduced. This can be the case if the power

* Corresponding author.
E-mail addresses: ruben.mocholi.montanes@sintef.no (R.M. Montañés), adriana.r.lua@sintef.no (A. Reyes-Lúa).

https://doi.org/10.1016/j.energy.2024.130315
Received 24 August 2023; Received in revised form 3 January 2024; Accepted 8 January 2024
Available online 13 January 2024

Nomenclature

Abbreviations

1D	One dimensional
C_i	Operational constraint i
$CO_{2,eq}$	CO_2 equivalent, kg or t
$CO_{2,int}$	CO_2 intensity, $kg\,MJ^{-1}$
$CO_{2,tot}$	CO_2 total, kg or t
CCGT	Combined cycle gas turbine
CV	Controlled variable
DAE	Differential–algebraic equation
DV	Disturbance variable
FMI	Functional mock-up interface
FPSO	Floating production storage and offloading
GHG	Greenhouse gas
GT	Gas turbine
HRSG	Heat recovery steam generator
IAE	Integral absolute error
LHV	Lower heating value
MPC	Model predictive control
MV	Manipulated variable
NASA	National Aeronautics and Space Administration
NCS	Norwegian Continental Shelf
OTSG	Once-through steam generator
PID	Proportional–integral–derivative (controller)
PI	Proportional–integral (controller)
SIMC	Simplified internal model control (PID tuning rules)
SISO	Single-input single-output (controller)
ST	Steam turbine
VGV	Variable guide vane
WHRU	Waste heat recovery unit

Symbols

η	Efficiency, %
ρ	Density, $kg\,m^{-3}$
τ_c	Closed loop time constant, s
τ_I	Integral time constant, s
θ	Valve opening, %
c_p	Specific heat capacity, $kJ\,kg^{-1}\,K^{-1}$
d	Disturbance
H	Specific enthalpy, $kJ\,kg^{-1}$
K_c	Controller gain
m	Flowrate, $kg\,s^{-1}$
p	Pressure, bar
T	Temperature, °C or K
u	Input
v	Transformed input
W	Power, MW_{el}
w	Additional measured or estimated states
y	Output (vector)
z	Transformed output

produced by one gas turbine is instead provided by (i) a steam turbine in a bottoming cycle, and (ii) by increasing the load, and efficiency, of the remaining gas turbines [6,10–12].

Despite large combined cycles are standard for onshore power generation, it is important to highlight that the installation of *compact* combined cycles offshore is not a widespread practice [3] and there are few examples of installed cycles. In the NCS there are bottoming cycles installed and in operation in Oseberg (since 1999) [4,13], Eldfisk in the Ekofisk area (since 1999) [4,13,14], and Snorre B (since 2000) [4,13]. More recently, a combined cycle power plant was installed in the Appomattox production platform in the Gulf of Mexico [15]. The floating production storage and offloading (FPSO) vessel for the Bacalhau field offshore Brazil will use a combined cycle heat and power cogeneration system [16]. These recent installations are driven by the need to reduce emissions from offshore operations [3,17]. However, with a limited deployment, challenges and optimization opportunities still remain with respect to design and efficient operation of compact combined cycles offshore [10–13,18].

The most important aspects limiting a widespread deployment of steam bottoming cycles in offshore installations are weight and space availability, especially for retrofitting cases. A strategy to minimize weight and volume is to install one-pressure-level bottoming cycles, with compact once-through stream generators (OTSG) with small tube diameter as HRSG [11,12,19,20]. Some aspects of control of onshore combined cycles may be translated to offshore cycles. However, compact combined cycles require dedicated analysis because the dynamic response and operation of the compact bottoming cycle is largely determined by the response of the compact OTSG, a single heat exchanger for all three phase regimes. To the authors' knowledge, there are few studies focused on control of compact offshore combined cycles with steam bottoming cycles. Nord and Bolland [21] studied the off-design performance of different configurations of offshore combined cycles and the effect of steam pressure. More recently, Montañés et al. [10] analyzed the dynamic response of compact OTSGs, while Nord and Montañés [13] and Zotică et al. [22] compared control alternatives for compact bottoming cycles. Feedback control alone is sometimes not sufficient to achieve satisfactory disturbance rejection with changing power demand and feedforward control is required [10,13,22]. Moreover, the OTSG behaves nonlinearly. Zotică et al. [22] proposed a systematic approach using nonlinear input and output transformations for feedforward disturbance rejection for compact steam bottoming cycles.

This paper is built from and expands the scope of previous work [10,13,22], where the focus was on controlling the superheated steam temperature and comparing two operation modes for pressure control, i.e. constant and sliding pressure, and different control approaches. Before, the gas turbine exhaust had been considered as a boundary condition for the bottoming cycle, and the energy in the gas turbine exhaust was the main disturbance to the bottoming cycle. Here, we extend the system to include the gas turbines and analyze the control and operation of the compact combined cycle, still considering a compact steam bottoming cycle optimally designed with respect to weight while satisfying thermodynamic and process constraints, using the approach described by Skaugen et al. [20] and Montañés et al. [10].

This contribution examines the performance, operation, and control problem for an optimally designed compact combined cycle for offshore operation producing power only. This contribution is twofold and it concerns i) the effect of gas turbines' load allocation on the steady-state performance of the compact combined cycle, and (ii) a dynamic performance analysis of the combined cycle to large and sudden power demand changes.

The remaining of the paper is structured as follows. Section 2 describes the combined cycle process and model. Section 3 presents the operation problem of the combined cycle, and describes the control structures for gas turbines' load allocation and for steam temperature and pressure control which are then applied in a numerical case study in Section 4. Finally, Section 5 concludes the paper by pinpointing the contributions and potential impact of the work.

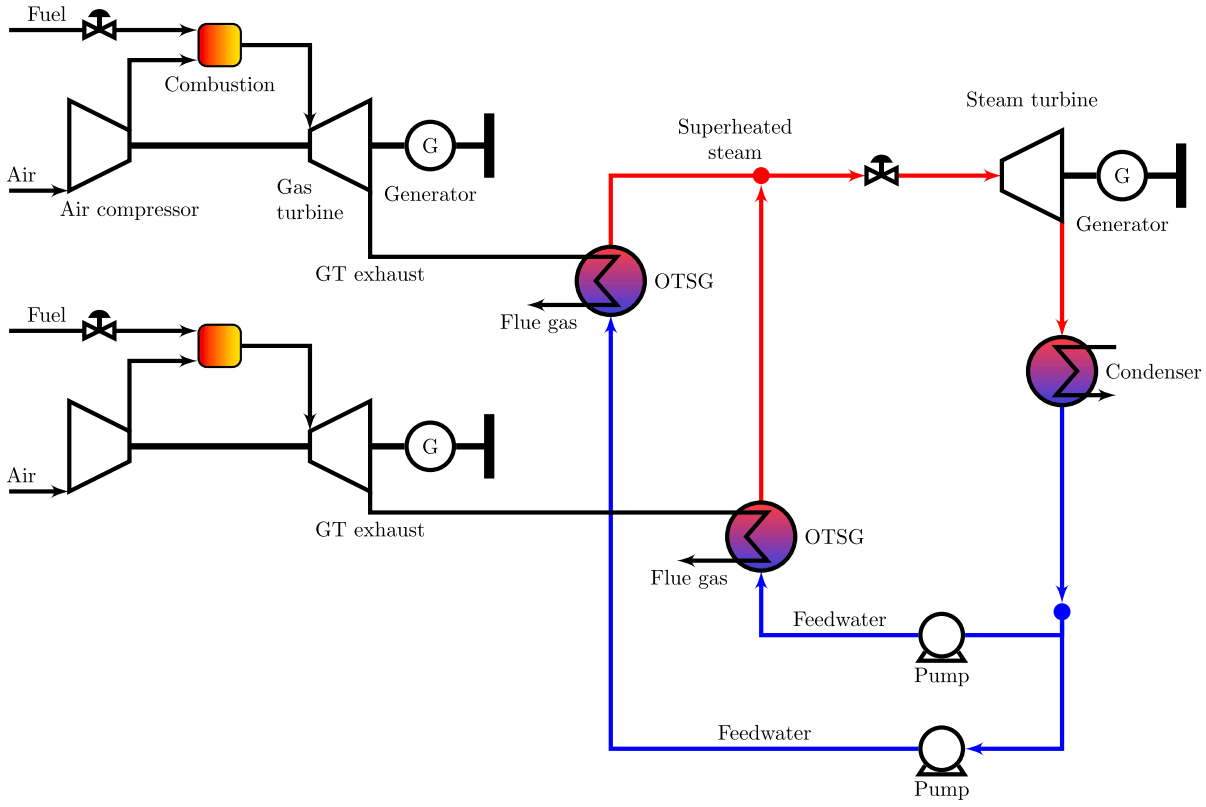

Fig. 1. Simplified process flowsheet of a compact combined cycle with a steam bottoming cycle recovering heat from two gas turbines to produce superheated steam in two once-though steam generators (OTSG), which is then expanded in a condensing steam turbine to produce power.

2. Offshore combined cycle: process and model description

2.1. Process description

Fig. 1 shows a simplified process flowsheet of the system considered in this work. This is a "standard" configuration in offshore installations, with two gas turbines and one steam turbine. For each of the gas tubines, there is an OTSG producing superheated steam that is fed to a common steam turbine [10,12,23,24].

Natural gas is burned with compressed air in a predefined ratio producing high-pressure and high-temperature gases which are then expanded. The exhaust heat from each gas turbine is recovered in a compact OTSG by generating superheated steam. High-pressure feedwater enters each OTSG, where it is heated, evaporated, and superheated in a single heat exchanger with small tube diameter, significantly reducing the size of the system compared with typical onshore steam cycles [19,24]. The superheated steam from both OTSGs is mixed and fed to a common steam turbine, where the steam is expanded driving a generator to produce electricity. The low-pressure steam is condensed using seawater as utility. The condensed and slightly subcooled feedwater is split between two variable speed pumps that boost the pressure and return the feedwater to the compact OTSGs. In this work, we do not consider an exhaust gas bypass stack to further reduce the system's weight and volume footprint.

2.1.1. Design characteristics of the analyzed process

Table 1 shows the main characteristics of the gas turbines at the design point [25], while Table 2 summarizes the nominal operating conditions for the steam cycle [22], which is designed for the case when both gas turbines operate at their design point, i.e., 90% load. With this, at the nominal point the combined cycle power plant will provide a total power output of ca. 92 MW_{el}, i.e., ca. 36 MW_{el} from each gas turbine and 20 MW_{el} from the steam turbine.

Table 1
Design point characteristics of the Siemens SGT-750 gas turbines considered in this work [25,26]. The ambient ISO conditions are 15 °C, 1 bar and 60% relative humidity.

Variable	Unit	Value
Power output	MW_{el}	39.8 (35.8 @ 90% load)
Fuel		Natural gas
Frequency	Hz	50/60
Gross efficiency	%	40.3
Heat rate	$kJ\,kW^{-1}\,h$	8.922
Turbine shaft speed	rpm	6100
Pressure ratio	–	24.3:1
Exhaust mass flow	$kg\,s^{-1}$	115.4 (112.6 @ 90% load)
Exhaust temperature	°C	468 (443.3 @ 90% load)
NO_x emissions	ppmv	<9

Table 2
Nominal operating conditions for the compact steam bottoming cycle [22].

Variable	Unit	Value
Steam turbine power output	MW_{el}	20
Superheated steam pressure	bar	23
Superheated steam temperature	°C	353
Exhaust gas inlet temperature	°C	443
Exhaust gas outlet temperature	°C	169
Cooling water temperature	°C	12
Feedwater inlet temperature	°C	27
Feedwater mass flowrate	$kg\,s^{-1}$	21.9
Exhaust gas mass flowrate	$kg\,s^{-1}$	225.5
Turbine valve opening	%	90

There are several aspects of operational flexibility from a power plant operation perspective. In the long term, power plants offshore need to operate flexibly to cover a wide range of total combined cycle power output demand. The operating window is normally defined as a range between maximum power load, and minimum compliant load. The SGT-750 turbine manufacturer guarantees low emissions down to

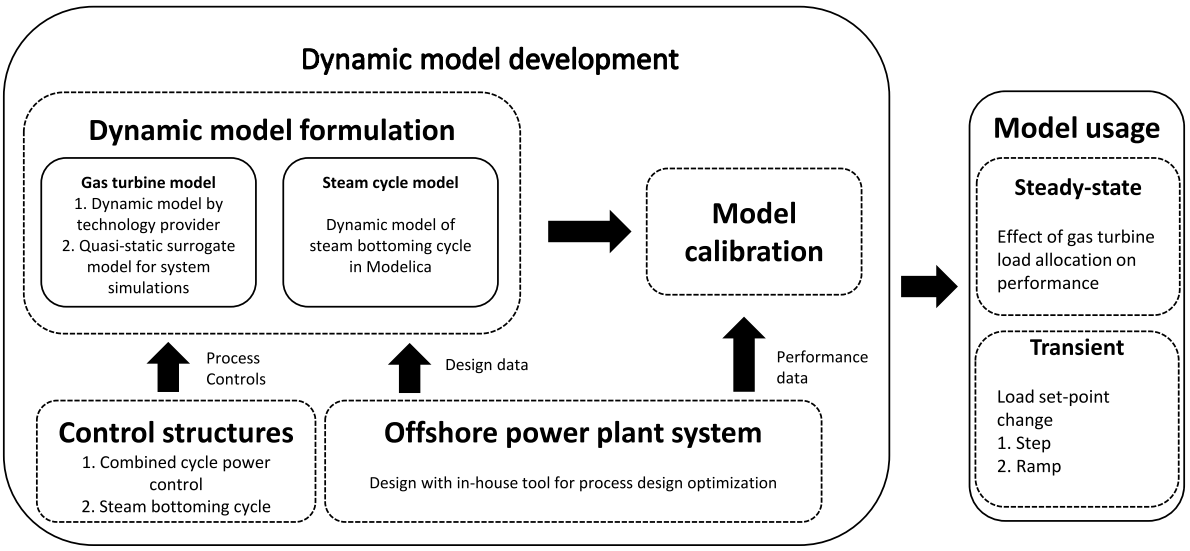

Fig. 2. Simulation tools and methods used for the dynamic model of the compact combined cycle.

20% gas turbine load (ca. 8 MW_{el}) for this turbine in single cycle mode. When a power plant needs to operate on a wide range of loads over the course of weeks or lifetime, the steady-state operational efficiency at different loads becomes crucial to save fuel and reduce specific CO_2 emissions. This is simulated and analyzed in Section 4.1. Specific emissions normally increase at part load in thermal power plants, and drastically in aeroderivative gas turbines. In the shorter time scale perspective, the power plant should be able to change load on demand, as well as provide reserve capacity to accommodate variability in power demand, both for planned and unplanned load setpoint changes. These simulations are presented and studied in Section 4.2.

2.2. Dynamic model of the combined cycle

We implement the dynamic model of the combined cycle in the Modelica language and Dymola simulation environment [27], using component models from the Thermal Power Library [28] as basis for process model development. The main subsystems models of the combined cycle system are the gas turbines, the OTSGs, steam turbine and generator, feedwater pumps, condenser and valves, as shown in Fig. 1. We parameterize and initialize the models based on the equipment geometry, material, and thermodynamic states from the process design optimization. In addition, we implement both a regulatory and supervisory control, using continuous, discrete, logical, functions and table blocks. Fig. 2 provides an overview of the tools and methods used for developing the dynamic model used in this contribution.

2.2.1. Gas turbine model

The gas turbines are SGT-750 twin-shaft gas turbines with the design characteristics in Table 1. A proprietary validated dynamic model developed in Modelica was provided by the turbine developer, Siemens Energy, through the LowEmission Research Centre [29]. The model includes the core engine, the generator, the control system, and follows the principles presented by Raddum [25]. The model, as received from the turbine provider, is a functional mock-up interface (FMI), which is, in essence, a validated dynamic black-box model.

Due to the time-scale separation between the gas turbine and the bottoming cycle dynamics, the dynamic response of the gas turbine is approximated with a surrogate quasi-static model. The power response is instantaneous, while the exhaust gas temperature, flowrate and composition have a first-order response with a time-constant of 5 s. The gas turbine model implementation in this work is a look-up table, and the outputs capture the steady-state off-design part-load performance of the gas turbine in a range of 5% load to 100% load, including fuel requirements and therefore, emissions.

2.2.2. Steam bottoming cycle model

To model the fluid thermodynamic properties, we assume non-ideal behavior for water and steam, modeled using the IF97 standard [30], and ideal gas behavior for the exhaust gas, modeled using the NASA Glenn representation, with a 6^{th} order polynomial for individual species [31]. The detailed dynamic model of the compact OTSG and the design optimization method and its validation are described in detail in previous work by Montañés et al. [10]. The model is based on a one-dimensional (1D) approach for dynamic modeling and simulation of heat recovery steam generators as suggested by Dechamps [32].

For the steam turbine expansion we model the turbine section, not the individual stages. The model includes mechanical shaft efficiency, flow characteristics and constant isentropic efficiency with an efficiency degradation due to the steam turbine outlet vapor containing water droplets. Stodola's law of cones is used for the flow characteristics [33], based on nominal design point values for the coefficient. The model equations are the ones presented by Jonshagen and Genrup [34]. We disregard shaft inertia and it is a static model with no energy or mass storage.

The condenser model is a cylindrical condenser, assuming thermodynamic vapor–liquid equilibrium. Cooling water and steam/condensate are separated by a dynamic wall model. It is a 1-dimension model of a metal wall where the heat capacity is lumped at the center of the wall. The properties that mostly affect the transient are density – a higher value of the density increases the heat capacity and thereby the wall dynamics time constant – and thermal conductivity — a higher value of the thermal conductivity decreases the thermal resistance and thereby the wall dynamics time constant. The heat transfer equation on the steam side is a correlation for condensation over tube bundles suitable for system studies, while on the cooling media side it is a correlation that uses the logarithmic average of the cooling inlet and cooling outlet temperature as the driving force temperature. The condenser hotwell serves as a water reservoir for the bottoming cycle. During normal full load operation with nominal hotwell levels, the main condenser provides minutes of active condensate storage volume [35]. Based on this, we assume a residence time in the condenser hotwell of 5 min.

The inputs, outputs and operational constraints of the model which are relevant for process control are described in Section 3.

2.2.3. Model validity

The dynamic model of the SGT-750 gas turbine was provided by the gas turbine vendor and is verified with proprietary data, as described

by Raddum [25]. The surrogate quasi-static model of the gas turbine developed in this work simulates the same steady-state part load performance as the gas turbine dynamic model for the operating window of interest.

The steam bottoming cycle design used in this work represents a *compact* system that has not been put in operation and for which there is no operational data available for direct comparison or validation. In this work, we parameterize the dynamic process models with process and equipment geometry data from a reference cycle designed by means of an in-house tool for process design optimization of offshore compact bottoming cycles. We use data from the design tool to calibrate the dynamic model and verify the model performance. The underlying design models and the optimization routines are described by Montañés et al. [10],Montañés et al. [11],Mazzetti et al. [12]. The underlying OTSG design model is most thoroughly presented in [10] (refer to supplementary material of [10]), where it was validated against industrial boiler data from Dumont and Heyen [36]. The rest of the dynamic component models of the combined cycle build from a Modelon AB [28] component library, thoroughly validated in the literature with steady-state and dynamic data [13,37–39].

In addition, the underlying dynamic process models of the steam bottoming cycle were previously validated by Nord and Montañés [13] using as reference an existing offshore combined cycle and with data from the installations at the Oseberg Field Center with OTSGs installed in 2011–2012. The results from Nord and Montañés [13] show the capabilities of the dynamic process model to capture the steady-state performance of the process at close to the design point, and for several steady-state off-design gas turbine loads describing the whole operating window of the process (100% down to 20% gas turbine load). The off-design steady-state validation work consisted of software-to-software validation against the commercial software Thermoflow.

Based on the model implementation and verification in this work the dynamic models are suitable for simulation studies at the plant scale, including dynamic process simulations to analyze the plant transient behavior, and for control tuning and advanced control layer design, including control structure studies. It should be noted that unknown dynamics and plant-model mismatch (i.e., the difference of dynamics between the model built for the design and that of the current plant [40]) as well as unmeasured disturbances can be dealt with effectively using a well-tuned PI feedback controller [41,42]. Here, we use the SIMC tuning rules, which assure robustness [43,44]. Therefore, the insights of this work regarding system behavior would still be valid for systems with the same topology, even if they are not the same system analyzed in Section 4.

3. Operation and control of the combined cycle

In this work, we decompose the control problem of the combined cycle into its two main components or subsystems, that is, the gas turbines and steam bottoming cycle.

3.1. Operational objective of the combined cycle

The control objective of the gas turbines is to produce the required load. This can either be mechanical power (for example if the gas turbine directly drives a compressor or pump), or electrical power at the desired frequency and voltage. Here, the focus is on power production and frequency stabilization. In other words, the load control should reduce the variation in shaft speed over the full range of shaft power.

The control objective of the steam bottoming cycle is to process a given amount of exhaust gas from the gas turbines while satisfying the operational constraints. The steam bottoming cycle has no steady-state degrees of freedom available that can be used to increase its power produced with a given steam temperature and pressure. Therefore, while increasing overall power production and efficiency, it acts as a load disturbance to the gas turbines, which may be handled with feedforward control, as discussed in Section 3.4.

The operational objective of the combined cycle is to provide the required energy. This translates to power and, in some cases, heat using steam extraction. In this work we consider a cycle generating power only. Here, the total power output is the sum of the power produce by the two gas turbines and the steam turbine. This is further analyzed in Section 3.4.1.

3.2. Controlled variables, available manipulated variables, and main disturbances

The gas turbine control system is responsible for maintaining desired operation of the gas turbine through manipulating fuel and air flow [25]. The control system needs to measure and adjust temperatures and speed in order to deliver the required power but also reduce the wear of specific equipment parts. The control system of a gas turbine consists of several sensors, controllers and actuators in order to achieve optimal operation. The main sensor inputs are temperatures, pressures throughout different locations of the gas turbine and turbine shaft rotational speed [25]. The signals are compared to reference signals (setpoints) and the result is fed through a low signal selector and the actuators (MVs) controlling fuel valves and variable guide vanes (VGV). As we are using a validated proprietary model, we do not modify the internal controls of the gas turbine, and we use the gas turbine load setpoint as manipulated variable. Therefore, the gas turbine model has only one input, and therefore degree of freedom for operation, which is the load setpoint, u_1^{GT}.

The outputs of the gas turbine model are:

y_1^{GT} : fuel mass flow rate [$kg\,s^{-1}$]

y_2^{GT} : exhaust gas mass flowrate [$kg\,s^{-1}$]

y_3^{GT} : exhaust gas temperature [°C]

y_4^{GT} : exhaust gas mass concentrations of CO_2, H_2O, N_2 and O_2

y_5^{GT} : power output [MW_{el}]

Table 3 identifies the manipulated variables (MV), controlled variables (CV) and main disturbances (DV) used in this work for the combined cycle. Note that from a system perspective, the gas turbine exhaust flowrate and temperature (DV2 and DV3) are not external disturbances because they are dependent on the fuel usage, and thus are internal states (variables) which affect the steam bottoming cycle. Also note that to maximize the produced power, the steam turbine bypass (MV4) is optimally closed and only used transiently to avoid too high pressure (C3 in Section 3.3), while the cooling water flowrate (MV5) is optimally completely open (C5 in Section 3.3). In this work, we consider constant ambient air conditions. In practice, air temperature, air pressure, or air humidity could be considered as disturbances that affect gas turbine performance.

3.3. Operational constraints (steady-state)

The operational constraints (C_i) for the steam bottoming cycle are systematically identified following a plantwide control approach described by Zotică et al. [45]. The identified CVs are a subset of the operational constraints of a drum-based heat-to-power cycle identified in [45].

C1. $T_s^{min} \le T_s \le T_s^{max}$: keep the superheated steam temperature, CV2 = T_s, at a given value to maximize the power extracted in the turbine, but within minimum and maximum allowed limits to prevent larger thermal gradients and stresses on the mechanical components or trigger steam turbine trips.

C2. $p_s^{min} \le p_s$: keep the superheated steam pressure, CV3 = p_s, above minimum allowed limit to avoid steam turbine trip.

Table 3
Manipulated variables (MV), controlled variables (CV) and main disturbances (DV) for the combined cycle.

Subsystem	MV	CV	DV
Gas turbine (model)	MV1=Power setpoint ($u_1^{GT} = W_{GT}^s$)	CV1=Total power (W)	DV1=Power demand
Steam cycle	MV2 = Feedwater flowrate (m_w) MV3 = steam turbine valve opening (z_T) MV4 = Turbine bypass opening (z_{TB}) MV5 = Cooling water flowrate (m_{cw})	CV2 = steam temperature (T_s) CV3 = steam pressure (p_s) CV4 = condenser pressure (p_c)	DV2 = gas turbine exhaust flowrate (m_g) DV3 = gas turbine exhaust temperature (T_g) DV4 = cooling water temperature (T_{cw})

C3. $p_s \leq p_s^{max}$: keep the superheated steam pressure, CV3 = p_s, below maximum limit to avoid high mechanical stresses on the mechanical components.
C4. $p_c^{\min} \leq p_c$: keep condenser pressure, CV4 = p_c, above minimum limit to avoid liquid droplets at the steam turbine outlet .
C5. $F_{cw} = F_{cw}^{\max}$: keep the cooling water flowrate, MV5 = F_{cw}, at maximum to maximize the pressure ratio over the steam turbine and maximize produced power.
C6. n=50 (60) Hz: keep the turbine speed at the setpoint. This is taken care of by the safety control layer, and it is therefore not included further in the supervisory or regulatory control system design in this work.

Furthermore, there are operational constraints on the gas turbine side, e.g., speed and inlet gas temperature. However, these are already handled by a lower control layer present in the gas turbine model supplied by Siemens and implicitly in the surrogate quasi-static model used in this work.

3.4. Analyzed control structures

We first describe the proposed control structures for load allocation and then summarize the control structures used for the steam bottoming cycle, which are described in detail by Zotică et al. [22].

3.4.1. Control structures for gas turbine load allocation

From a control point of view, the combined cycle is a system with one output, which is the total power ($y = W^{tot}$). The total power is the sum of the load of the two gas turbines (inputs $u_1 = u_{GT1}$ and $u_2 = u_{GT2}$) and the power produced by the steam turbine ($w = W^{ST}$). The power produced by the steam turbine is not an independent degree of freedom, at least not at steady-state and with constant temperature and pressure setpoints.

With two degrees of freedom, u_1 and u_2, the system in Eq. (1) is under-determined and we need to decide *a-priori* how to allocate the load between the two gas turbines.

$$y = u_1 + u_2 + w \tag{1}$$

In this work, we propose two control strategies for gas turbine load allocation:

1. Feedforward control, developed in the framework of the input transformation method [18] (Fig. 3(a)).
2. Feedback control, using one I-controller and one P-controller (Fig. 3(b)).

Feedforward, shown in Fig. 3(a). allocates the load equally between the two gas turbines because for this system, the two gas turbines are identical, see Eq. (2). For a general system, the load can be allocated proportionally to their rated (design) power output. Solving Eq. (1) for equal inputs $u_1 = u_2$ with given measured steam turbine output w and total power output y yields

$$u_1 = u_2 = \frac{y - w}{2} \tag{2}$$

There is a potential issue of internal instability when using a measurement dependent on the input u if the system has zero-dynamic (corresponding to right-half plane zeros or inverse response in the linear case). However, this is not the case in this system, where the response corresponds to an overshoot (left-half plane zeros in the linear case). Industrial control solutions often make use of nonlinear calculation blocks derived from steady-state model and applied to dynamic problems [46–48]. Guzmán and Hägglund [48], Hast and Hägglund [49] and Skogestad [46] give insights for alternatives for implementation of feedforward controllers under different scenarios. Here, we have a model and no risk of saturation, and feedforward as in Eq. (2) and Fig. 3(a) is sufficient.

Feedback, shown in Fig. 3(b). does not allocate the load equally between the two gas turbines. Both gas turbines participate dynamically to changes in load and allocation depends on the (dynamic) error between the total load, W^{tot}, and the load setpoint, W^s. At steady-state, the P-controller drives the corresponding gas turbine towards its nominal load, while the I-controller drives the second gas turbine to a new load. Also note that by using a P-controller with a desired setpoint for one gas turbine, Eq. (1) becomes determined. The integral action of the I-controller assures that there is no steady-state error and the overall energy balance in Eq. (1) is closed.

In summary, option 1 drives both gas turbines to the same load and efficiency, while option 2 keeps one gas turbine close to its nominal load, thus at maximum efficiency, and the second gas turbine produces lower power, thus is at a lower efficiency. It is not straightforward to determine which option is best with respect to overall efficiency and load variations. In this paper we analyze the steady state effect of implementing these simple strategies. An alternative would be to implement a more sophisticated optimization algorithm that takes into account the turbine efficiency at different loads.

3.4.2. Control structures for the steam bottoming cycle

To control steam temperature and pressure, we use the decentralized control strategies based on standard PID-controllers and nonlinear feedforward described by Zotică et al. [22]. The main control loops for the steam bottoming cycle are shown in Fig. 4.

We analyze two operational strategies for the superheated steam pressure, CV3 = p_s:

1. it can be left sliding, i.e., varying with the heat input, thus minimizing throttle losses [22,45], or
2. keep it at a constant setpoint, p_s^s, using the turbine valve, MV3 = z_T.

For constant pressure, we use a pure I-controller, because the pressure dynamics have a very small time constant ($\tau \to 0$). Using the SIMC tuning rules [43] and selecting a closed loop time constant $\tau_c = 5$ s, gives an integral gain $K_I = -0.08$.

To control the steam temperature, T_s, we use the feedwater flowrate, m_w. In all cases, we implement feedback control and a type of model-based nonlinear feedforward control, which uses input and output transformations [18,50,51]. This implementation is shown in Fig. 5, which corresponds to the input transformation block in Fig. 4. The advantage of this approach is that it transforms a nonlinear system, i.e., the OTSG, into a linear system (from v to $y = T_s$) that is decoupled and that also has feedforward disturbance rejection because it considers the disturbances, d, to the OTSG, i.e., inlet exhaust gas temperature, T_g^i, and mass flowrate, m_g.

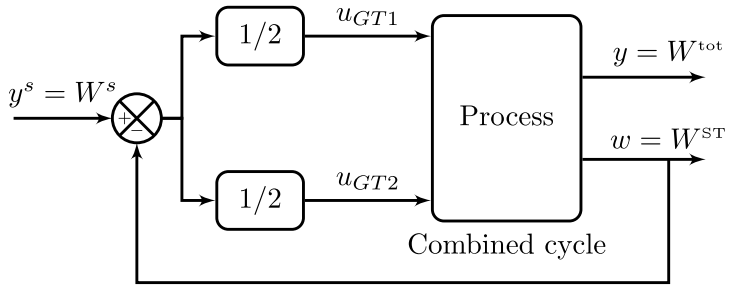

(a) Feedforward control: Equal load allocation between the two gas turbines.

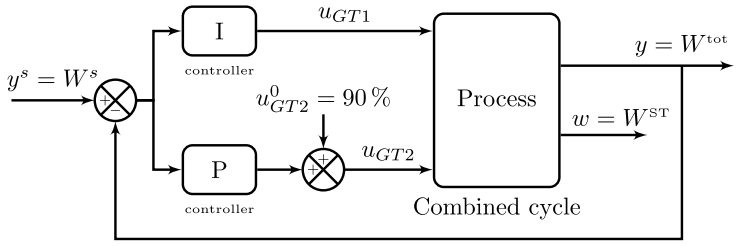

(b) Feedback control: After a load change, GT2 manipulated by with a P-controller participates dynamically, but at steady-state operates at nominal setpoint ($u^0_{GT2} = 90\%$). GT1 manipulated by an I-controller operates at a different load at steady-state after a load change.

Fig. 3. Block diagrams for two options for allocating the load (u_{GT}) between the two gas turbines: equal (a) and (b) not equal at steady-state. The Process block represents the combined cycle in Fig. 4.

In Fig. 5, the states are the water specific enthalpy and exhaust gas outlet temperature, $w = [H_w, T_g^o]$, and we assume that they can be measured or estimated. The steam enthalpy is a transformed output, $z = H_s$, and it can be estimated from measured pressure and temperature. The setpoint for H_s is computed similarly. Note that we use the pressure setpoint, p_s^s, for constant pressure operation and the measured pressure for floating pressure.

Zotică et al. [22] derived the inverted energy balance on Fig. 5 from the steady-state energy balance for the OTSG:

$$m_g c_{p_g}(T_g^i - T_g^o) = m_w \left(H_s - H_w\right) \tag{3}$$

The right hand side of Eq. (3) represents the phase change on the water/steam side of the OTSG and the left-hand side assumes constant specific heat for the gas, c_{p_g}.

The inverted energy balance in Fig. 5 is given by:

$$m_w = \underbrace{\frac{m_g c_{p_g}(T_g^i - T_g^o)}{v_0 - H_w}}_{f_{0z}^{-1}(v,w,d)} \tag{4}$$

We use an inner loop flow controller that manipulates the feedwater pump speed to keep the flow at its setpoint. This is a pure I-controller with a integral gain $K_I = 11.11$, tuned with a closed loop time constant $\tau_c = 5$ s, and is not shown in Figs. 4 and 5. To allow for the time scale separation, for the outer (slow) controller, C_1, depicted in Fig. 5, we use a closed-loop time constant $\tau_c = 60$ s. Using the SIMC tuning rules [43] the PI-controller has a gain $K_C = 5.7$ and an integral time constant $\tau_I = 280$ s.

It should be noted that for both OTSGs, the temperature setpoint, T_s^s is the same at all loads and equal to the design value in Table 2. However, each of the OTSGs has an individual feedwater pump and transformation block (Fig. 5) for controlling the (outlet) steam temperature of the corresponding OTSG.

4. Simulation results and discussion

As previously described in Fig. 2, we first analyze the steady-state effect of load allocation and then we analyze the transient behavior with load setpoint changes.

4.1. Effect of gas turbines load allocation on steady-state performance

We compare the steady-state performance for the two control structures for allocating the load between the two gas turbines. These are equal load allocation using feedforward (Fig. 3(a)) and not equal load allocation using one pure I-controller for GT1 and one P-controller with a setpoint at 90% for GT2 (Fig. 3(b)). In addition, the superheated steam in the bottoming cycle can be controlled for either constant or sliding pressure.

To assess the steady-state performance of the two control structures for gas turbine load allocation for constant superheated steam and sliding pressure operation modes, we compare the steady-state efficiency (Fig. 6(a)) and CO_2 specific intensity at different loads (Fig. 6(b)). The results in (Fig. 6(a)) show and confirm that the combined cycle efficiency drops at part load, regardless of the control structure implemented.

For both load allocation schemes, sliding pressure for live steam control leads to higher combined cycle efficiency. This can be observed in the whole operational window of the combined cycle, but is more evident at lower loads (combined cycle loads between 56 MW to ca. 75 MW).

Here, running one of the gas turbines at low load using a pure I-controller and the second one at 90,% load using a P-controller (not equal load, Fig. 3(b)), gives a lower combined cycle efficiency compared to operating both gas turbines at equal load. In this case study, at lower loads (combined cycle loads between 56 MW to ca. 75 MW), the combined cycle efficiency reduction with respect to the

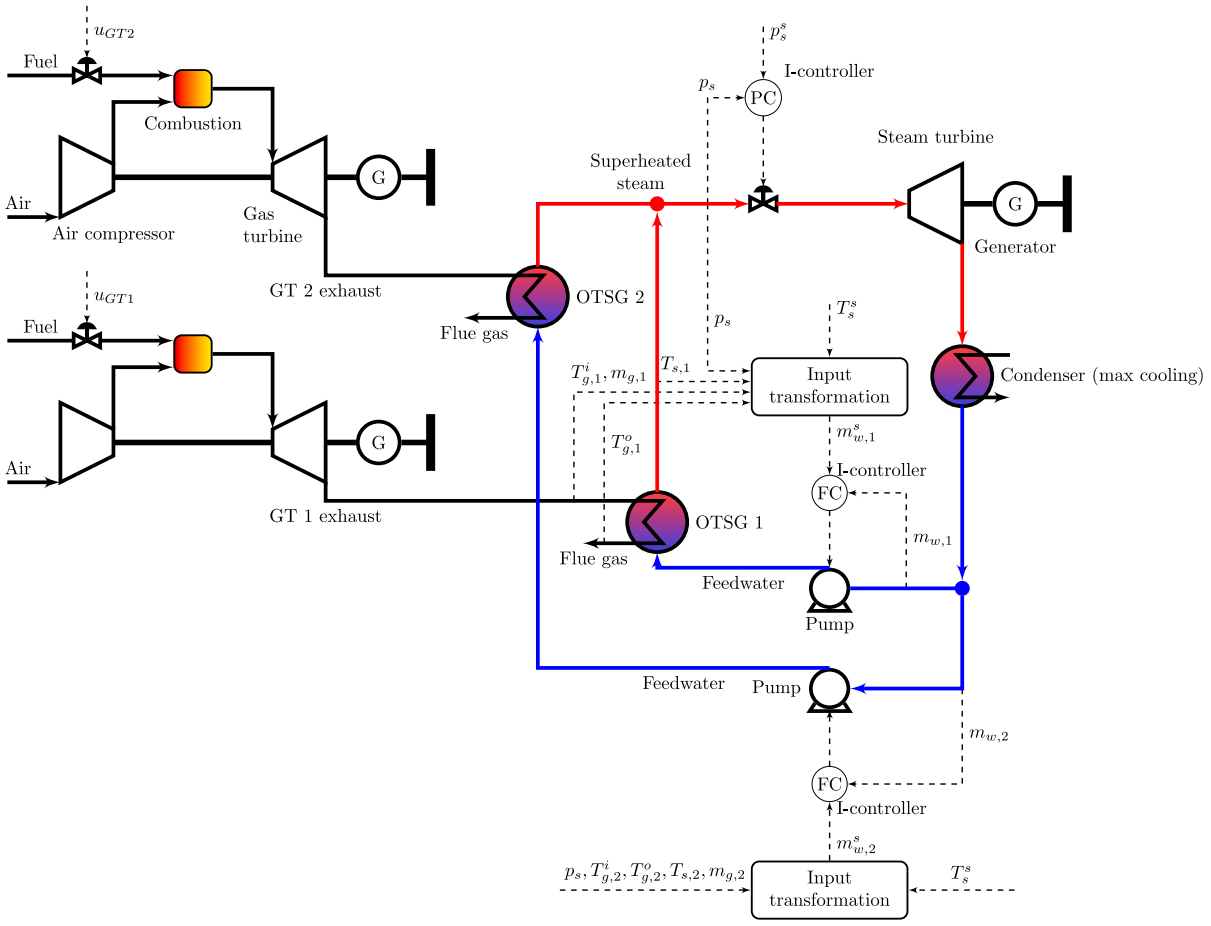

Fig. 4. Process flowsheet of the combined cycle (Process block in Fig. 3) showing the main control loops for the steam bottoming cycle. The input transformation block is shown in Fig. 5.

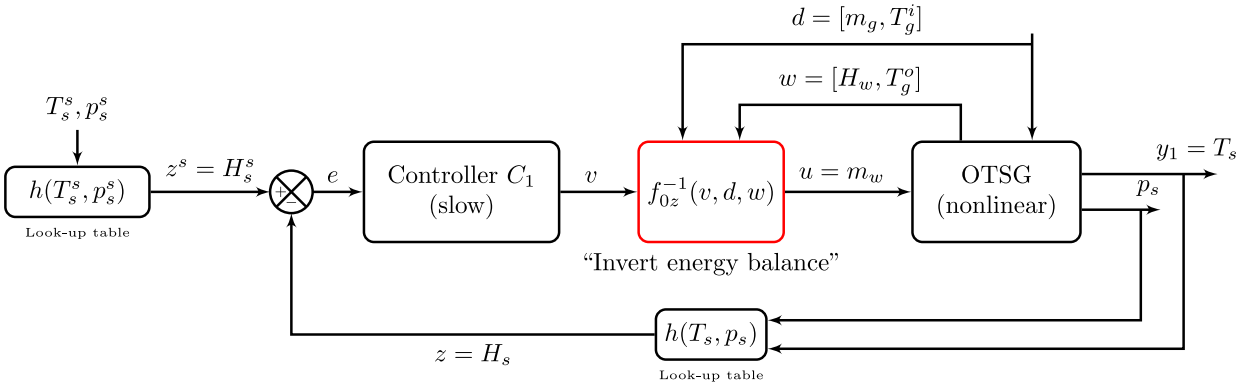

Fig. 5. Implementation of transformed inputs and outputs for steam temperature control.

efficiency at 90% load is significantly larger when the loads are not equal.

Fuel use and CO_2 specific intensity are related to the combined cycle efficiency, and lower specific emissions are achieved when selecting control structures that lead to higher efficiency. The results in (Fig. 6(b)) are in agreement with Fig. 6(a) and show that CO_2 specific intensity increases at lower loads. Accordingly, sliding pressure results in lower CO_2 specific intensity, both for equal load and non-equal load allocation of gas turbines load setpoint.

Fig. 7 illustrates the load allocation between the two gas turbines and the steam turbine for the operation strategy for both equal load (Fig. 3(a)) and not equal load allocation (Fig. 3(b)) and for both constant and sliding superheated steam pressure. The results show that the gas turbines combined provide ca. 80% of the total combined cycle power. There is also a small increase in the share of the load from the steam turbine at lower combined cycle loads.

Figs. 7(a) and 7(c) show that if the pressure is left uncontrolled (sliding pressure), the contribution of the steam turbine is larger, the reason being a reduction in throttling losses over the steam turbine. Moreover, the sharper combined cycle efficiency reduction at lower loads for not equal load distribution observed in Fig. 6(a), can be explained by observing the sharp load reduction of GT1 in Figs. 7(c) and 7(d) and the fact that the largest change in gas turbine efficiency

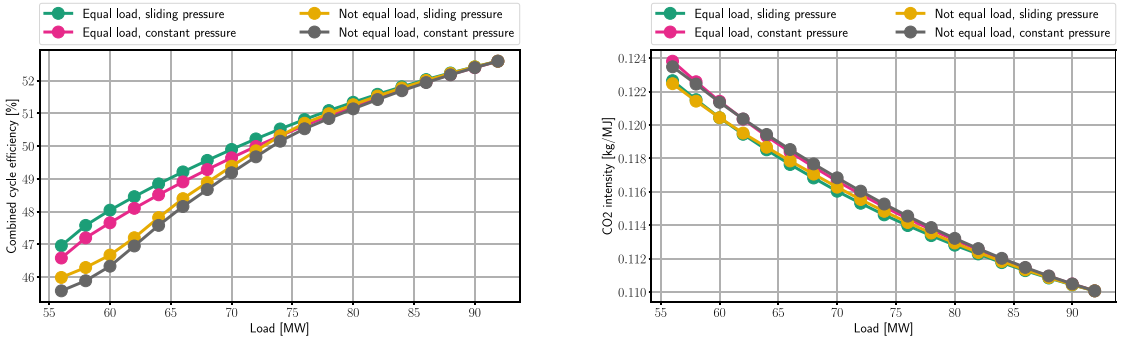

(a) Combined cycle efficiency (b) CO_2 specific intensity kg/MJ

Fig. 6. Steady-state performance comparison for the two control structures for allocation the gas turbines load with constant or sliding steam pressure operation respectively.

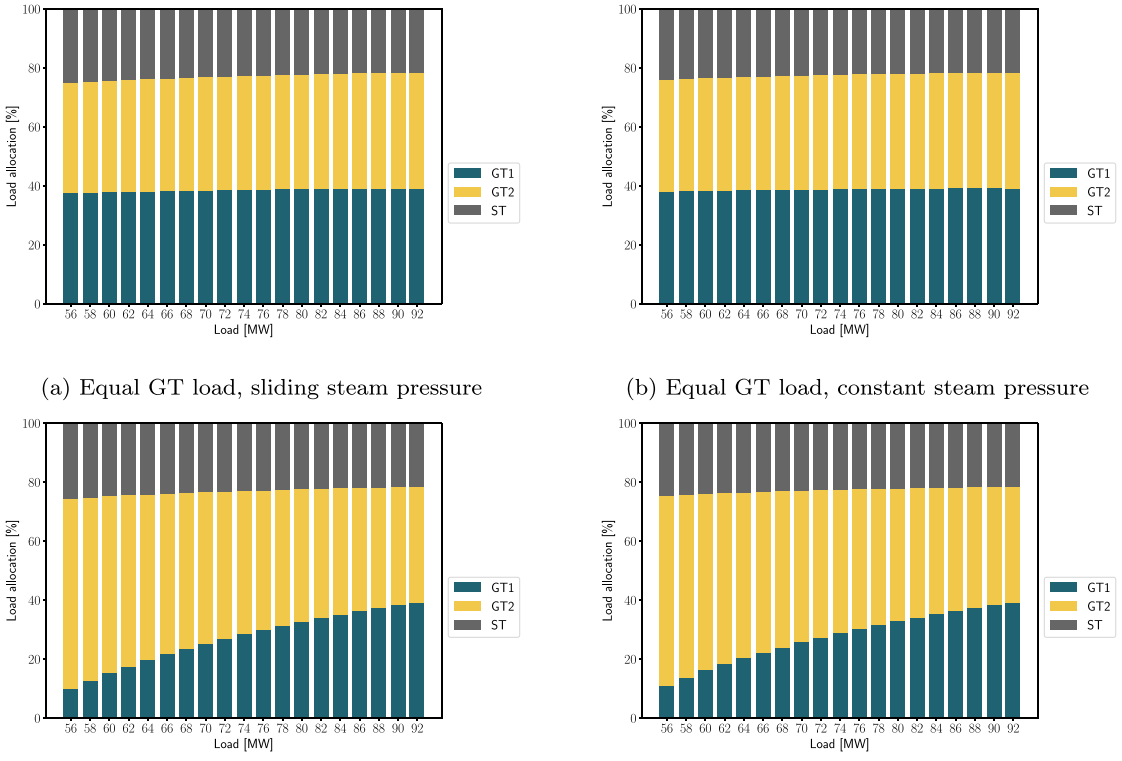

(a) Equal GT load, sliding steam pressure (b) Equal GT load, constant steam pressure

(c) Not equal GT load, sliding steam pressure (d) Not equal GT load, constant steam pressure

Fig. 7. Steady-state load allocation for the two gas turbines and steam turbine at different loads of the combined cycle for the four different control structures: equal gas turbine load in Fig. 3(a) and not equal gas turbine load in Fig. 3(b), with constant and sliding steam pressure.

is at low loads, while at higher loads, the change in efficiency flattens out.

To better understand the physics of the OTSG for operating under the two control structures for load allocation, in Fig. 8 we show the distribution of the water/steam phases (i.e. liquid, two-phase, and superheated steam) for the two OTSGs. The distribution is expressed as the estimated accumulated percentage of OTSG tube length having the specified phase. For all operation modes and loads, at steady-state all three phases are present and the outlet fluid is superheated steam, thus not imposing additional limitations on the steam turbine operation. The superheated region is the one with smaller total size, less than 20% in all control modes and loads. The results in Fig. 8 suggest that the superheated region size increases at part load, which is on the safe side to avoid droplet carry over to the inlet of the steam turbine.

Finally, Fig. 9 compares the steady-state steam sliding pressure values at different loads of the gas turbines for the two control structures for allocating the load. Except for the nominal operating point at 92 MW power output, the pressure is lower for equal load allocation. This reduces the throttling losses in the valve before the steam turbine, which increases the efficiency of the combined cycle.

It should be noted that, as described in Section 3.4.2, in all cases, the feedwater flowrate to each of the OTSGs is controlled to maintain the superheated steam temperature at the design value. For the constant pressure cases, the superheated steam pressure is also unchanged for all load demands. A possibility to improve the system performance could be to implement an upper supervisory control layer providing optimal setpoints, i.e., advanced control structures with self-optimizing controlled variables [52–54] or MPC, such as the one proposed by Qiu

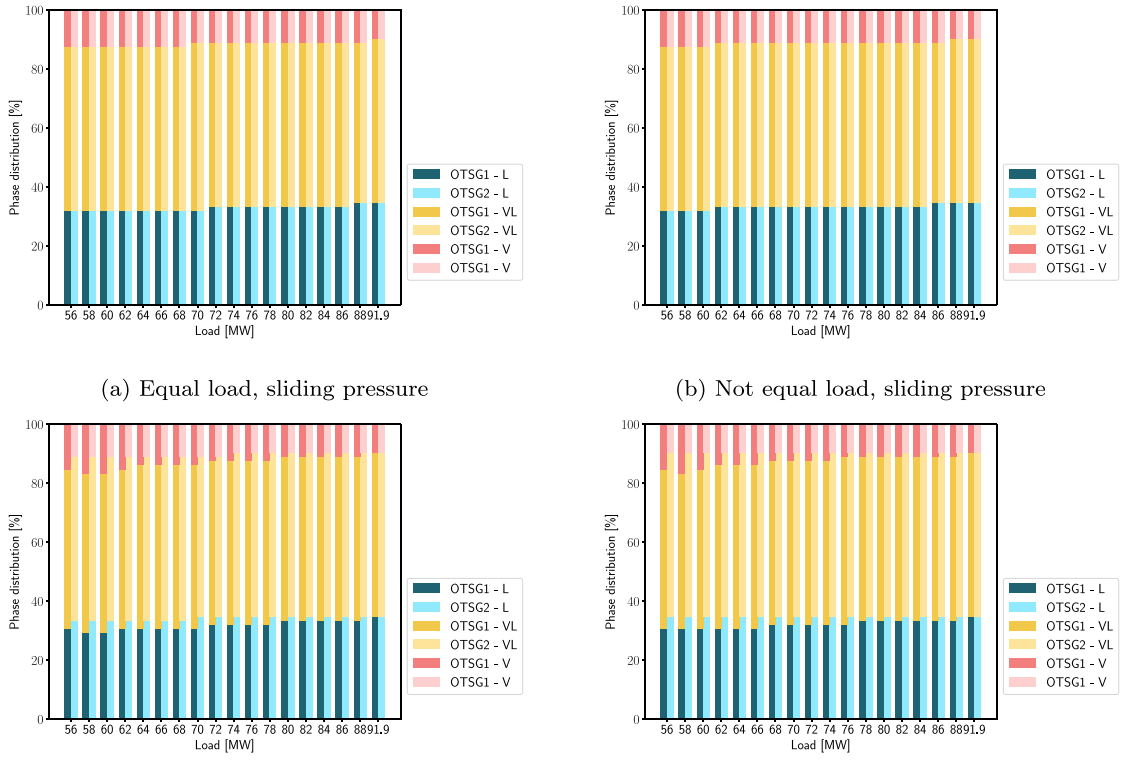

(a) Equal load, sliding pressure

(b) Not equal load, sliding pressure

(c) Equal load, constant pressure

(d) Not equal load, constant pressure

Fig. 8. Steady-state distribution of phase regimes in the two OTSGs at different loads of the combined cycle for the four different control structures: equal gas turbine load in Fig. 3(a) and not equal gas turbine load in Fig. 3(b). Liquid water in blue, two-phase in yellow, and superheated steam (vapor) in red. (For interpretation of the references to color in this figure legend, the reader is referred to the web version of this article.)

et al. [55] for offshore combined cycles. This is however out of the scope of this contribution.

4.2. Dynamic responses to load setpoint changes

Here we analyze transient scenarios for load change in total combined cycle load. When considering load change scenarios, there are always trade-offs, such as the one between input usage and fast load setpoint tracking. Reducing load fast might save fuel (as you reach a lower steady-state operational point faster), while in principle the opposite applies when ramping up. Also, in future offshore energy systems, e.g. including wind turbine parks, it might be relevant to enable fast load changes to balance the non-dispatchable power generation profiles of renewables [55], but this would also be at the expense of a higher input usage of the gas turbines.

In this work, we compare the dynamic response of sliding and constant steam pressure operation. For both cases, we consider equal load allocation of the gas turbines (Fig. 3(a)), which showed a higher combined cycle thermal efficiency in Section 4.1.

Under normal operation, thermal power plant operators commonly vary load implementing a ramp setpoint change for the total combined cycle power output. Operational eventualities, such as a trip in direct drive electrical motors, might lead to a sudden and automatic change in combined cycle load setpoint, which is represented as a step change in the combined cycle load setpoint. To analyze both scenarios, we simulate step changes and 5 MW/min ramp changes in the combined cycle load setpoint, both for load reduction and load increase. We consider two main magnitudes for load change, both for step and ramp setpoint changes on combined cycle power output setpoint:

1. A change from the nominal 92 MW_{el} to 77 MW_{el} (i.e. 15 MW_{el}). This represents an unplanned trip of large direct drive electrical motors.

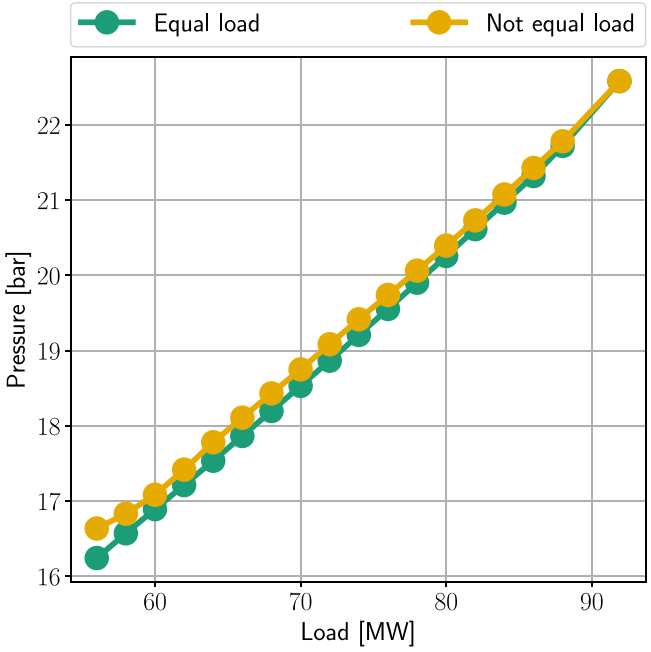

Fig. 9. Steady-state steam pressure for different combined cycle load with sliding pressure control implementation.

2. A change from the nominal 92 MW_{el} to 46 MW_{el} (i.e. 46 MW_{el}). We do this to explore the transient response of the system to larger load changes to the offshore energy system.

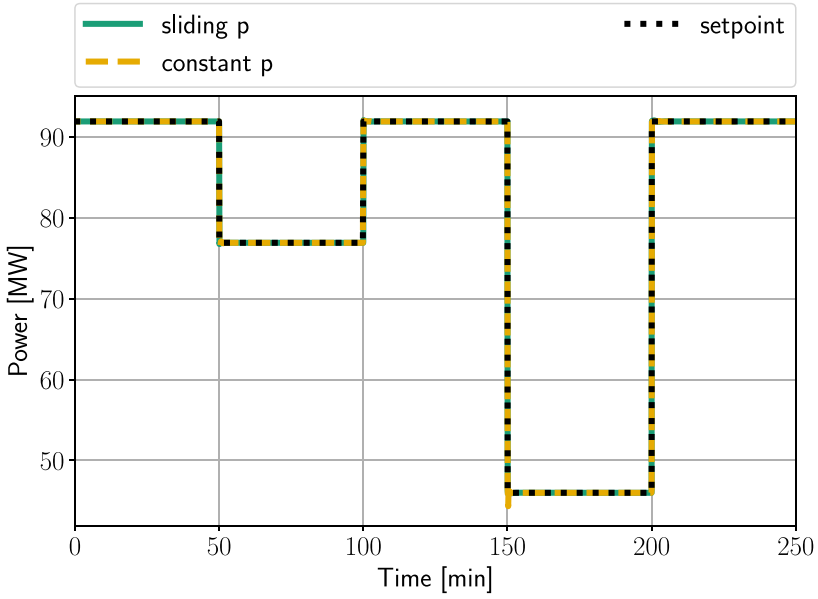

Fig. 10. Combined cycle power response to step changes in the load from 92 MW to 77 MW at time 50 min, back to 92 MW at time 100 min, to 46 MW at time 150 min and finally back to 92 MW at time 200 min.

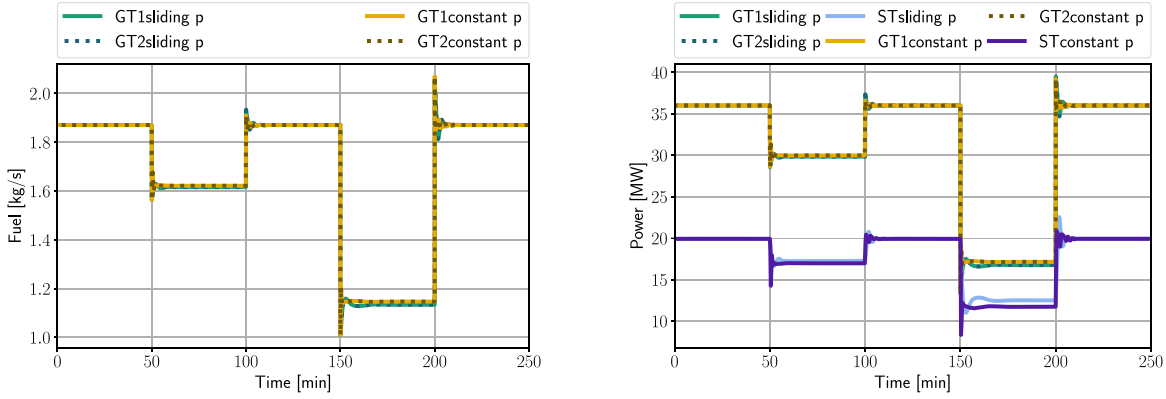

(a) Fuel response for both GT to a step changes in the load.

(b) Power responses for the two GT and ST

Fig. 11. Fuel and power responses to step changes in the load from 92 MW to 77 MW at time 50 min, back to 92 MW at time 100 min, to 46 MW at time 150 min and finally back to 92 MW at time 200 min.

4.2.1. Dynamic response to step changes in load setpoint

Fig. 10 shows the combined cycle total power output setpoint and response to step changes, while Fig. 11 shows the dynamic fuel response for the two gas turbines, and the power output for the three turbines respectively. The results in Fig. 10 show a perfect power output response dynamically because we use feedforward to allocate the load with perfect plant model knowledge (see Section 3.4.1). Moreover, there are negligible dynamics from the fuel input to the gas turbine power output, and the response becomes a pure static response, as shown in Fig. 11.

Fig. 12 shows the dynamic response for the feedwater flow rate and superheated steam temperature for both OTSGs. As mentioned earlier, each OTSG has an independent feedwater control, but both have the same temperature setpoint. Fig. 13 shows the dynamic response for the steam valve and pressure for both constant and sliding pressure operation modes. For sliding pressure (green line), the steam valve is kept open at 90% to reduce throttling loses. For constant pressure, the steam valve reaches saturation at about 100 min and 200 min, and we momentarily loose control of pressure. However, the deviation from the setpoint is not significant and control is regained fast. The controller has antiwind-up implemented using the back-calculation method which tracks the plant inputs (i.e., saturated valve) [56]. Keeping the pressure at constant setpoint results in faster power and temperature response to disturbance rejection. The reason is that the steam valve used to control the pressure has a direct effect on the steam turbine power output, corresponding to a left-hand plane zero. Moreover, this has a linearizing effect by reducing the deviations from the nominal point of the superheated steam enthalpy, which is a nonlinear function of temperature and pressure. In Fig. 12(b), it can be seen that this controller implementation could be sufficient to satisfy operational constraint C1 during transients. This is, to keep the superheated steam, T_s, within minimum and maximum allowed limits to prevent larger thermal gradients and stresses on the mechanical components or trigger steam turbine trips, as described in Section 3.3.

4.2.2. Dynamic response to ramp changes in load setpoint

Figs. 14–17 show similar response to a ramp load change with a rate of 5 MW/min compared to step changes. A perfect combined

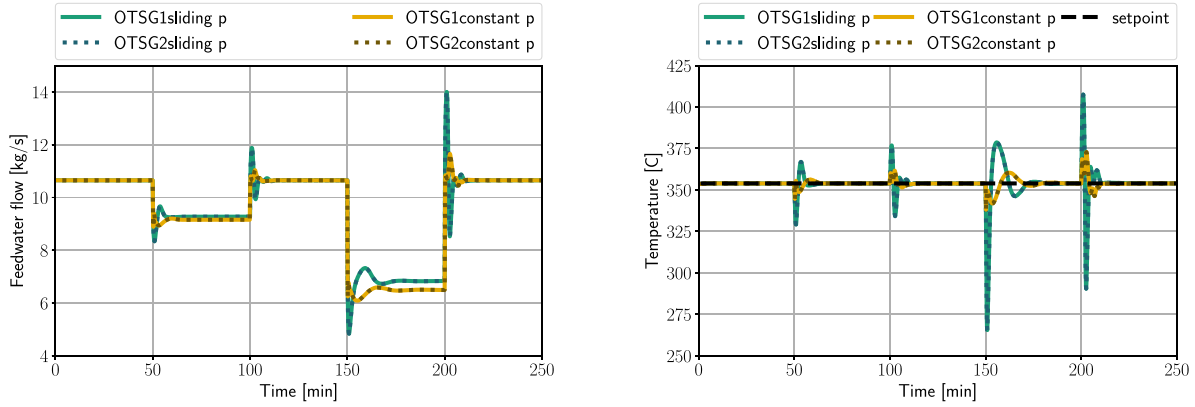

(a) Feedwater response for both OTSGs.

(b) Temperature response for both OTSGs.

Fig. 12. Feedwater and steam temperature responses to a step change in the load to step changes in the load from 92 MW to 77 MW at time 50 min, back to 92 MW at time 100 min, to 46 MW at time 150 min and back to 92 MW at time 200 min.

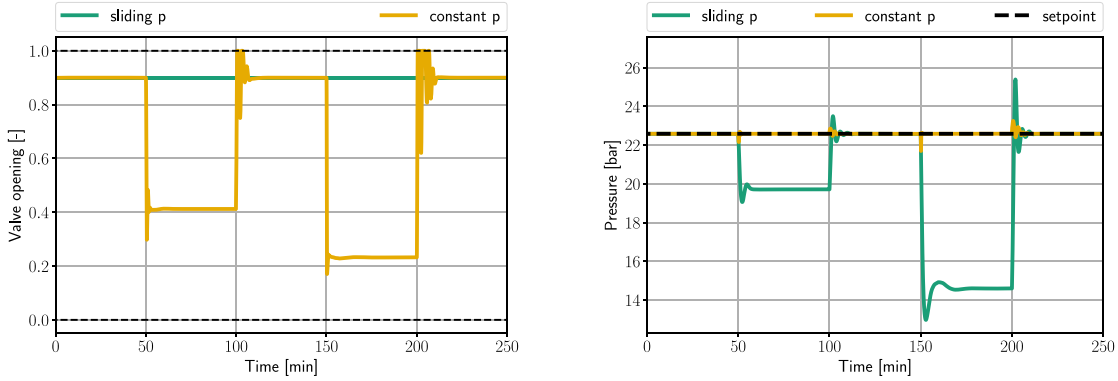

(a) Steam valve response to a step change in the load.

(b) Pressure response to a step change in the load.

Fig. 13. Steam valve and pressure responses to a step change in the load to step changes in the load from 92 MW to 77 MW at time 50 min, back to 92 MW at time 100 min, to 46 MW at time 150 min and finally back to 92 MW at time 200 min.

cycle power output response dynamically is observed in Fig. 14. The main difference, compared to step changes, is observed in the live steam temperature and pressure trajectories as shown in Fig. 16 and Fig. 17(b). When the gas turbine load is changed slowly in a ramp, the oscillations in live steam temperature are significantly reduced. The oscillations around setpoint in live steam temperature become similar in amplitude for sliding pressure and constant pressure control. This may be because with a smaller rate of change in gas turbine load the OTSG live steam temperature can follow more closely the trajectory of the gas turbine exhaust temperature. Therefore, the steam valve pressure controller follows the variations in feedwater flow rate input setpoint of the non-linear feedforward controller, and the resulting steam flow rate. This is, the plant (gas turbine and bottoming cycle) becomes more interactive as the rate of change of gas turbine load (and exhaust gas conditions) gets closer to the closed-loop time constant of the OTSG. This is consistent with the behavior observed in the work by Montañés et al. [10].

4.3. Evaluation of CO_2 specific intensity

We use the CO_2 specific intensity ($CO_{2,int}$), Eq. (5), of the generated power to compare the effect on GHG emissions of the control alternatives analyzed in this work.

$$CO_{2,int} = \frac{CO_{2,tot}}{W_{tot}} \quad [kg/MJ] \tag{5}$$

Table 4
Cumulative CO_2 specific intensity for step and ramp load changes for constant and sliding steam pressure operation and equal load allocation.

Load change	Pressure control	$\int_0^{250} (CO_{2,int})\, dt$
Ramp	Constant	90.75
	Sliding	90.52
Step	Constant	90.79
	Sliding	90.55

Here, W_{tot} is the total power produced by the combined cycle. $CO_{2,tot}$ is the total CO_2 direct emissions from the combustion process, and it is an output of the gas turbine model.

To compare the performance to load changes of the proposed control structures with equal load allocation for the two gas turbines, we use the integral of the $CO_{2,int}$. Table 4 shows the results for ramp and step changes for constant and sliding steam pressure control of the simulations in Section 4.2, from $t = 0$ min to $t = 250$ min.

Consistently with the higher combined cycle efficiency for sliding pressure control observed in Section 4.1, this control approach results in lower accumulated emissions, $\int_0^t (CO_{2,int})\, dt$. However, for the same pressure operation mode, the differences between step and ramp load changes are very small and are within the error for the numerical integration using the trapezoidal method.

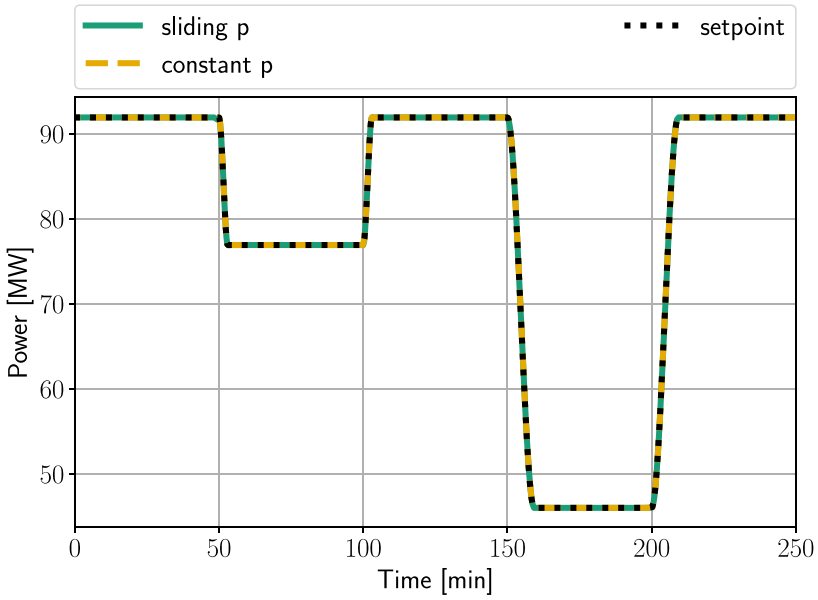

Fig. 14. Power response to ramp change in the load.

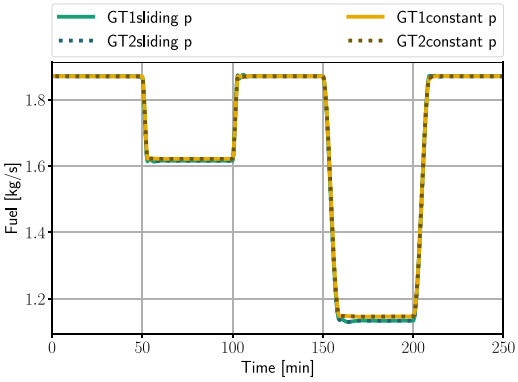

(a) Fuel response for both GT to ramp changes in the load.

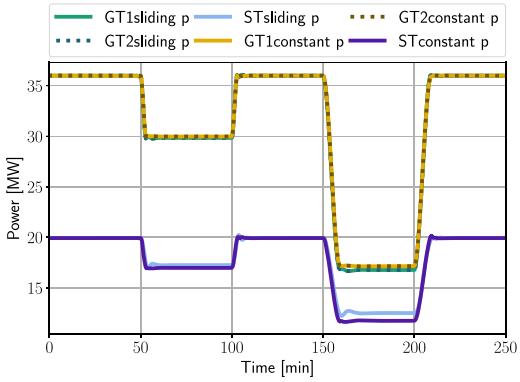

(b) Power response for both GT and ST to ramp changes in the load.

Fig. 15. GT and ST responses to ramp changes in the load.

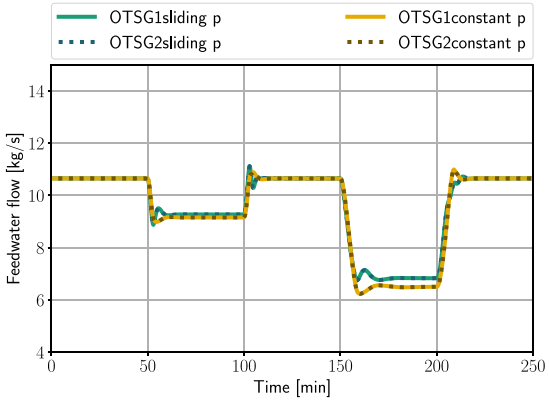

(a) Feedwater response for both OTSGs to ramp changes in the load.

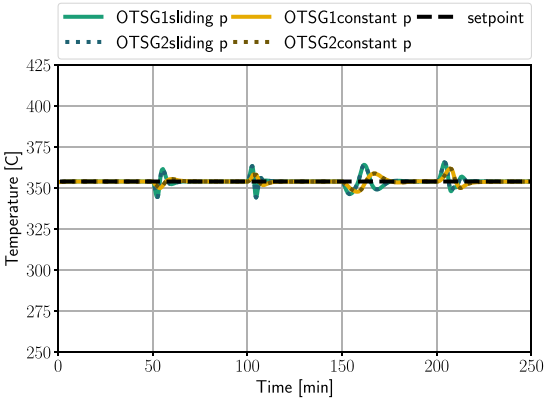

(b) Temperature response for both OTSGs to ramp changes in the load.

Fig. 16. Feedwater and steam temperature responses to ramp changes in the load.

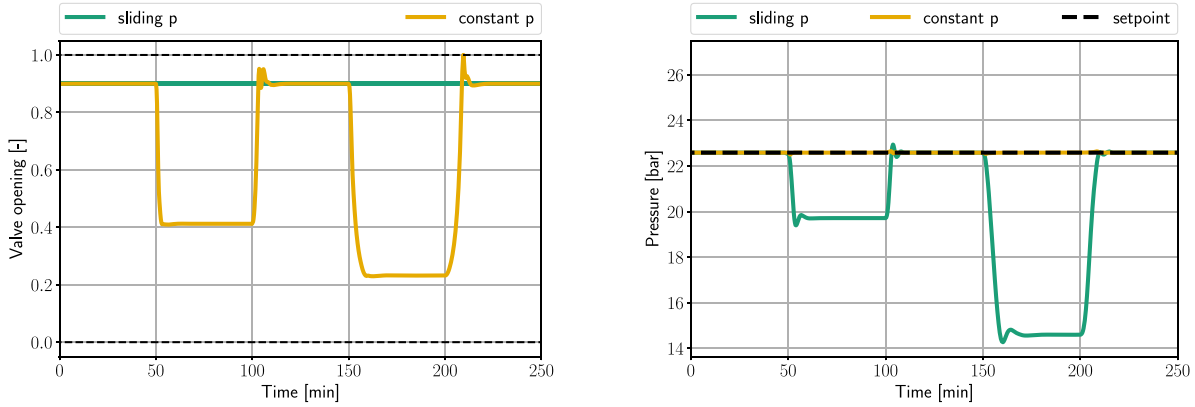

(a) Steam valve response to a step change in the load.

(b) Pressure response to ramp changes in the load.

Fig. 17. Steam valve and pressure responses to ramp changes in the load.

4.4. Summary and discussion of results

Here we highlight some findings of the steady-state and dynamic analysis. With respect to steady-state performance, allocating the load equally between the two gas turbines using pure feedforward (Fig. 3(a)) has higher efficiency as well as lower fuel consumption and CO_2 emissions compared to keeping one gas turbine close to nominal operation at 90%, and letting the second gas turbine to handle the load variation (Fig. 3(b)). As noted in Section 4.1, the reason is that gas turbines have an important reduction in efficiency at low load, and the gas turbine handling load variations is operating at a very low load when the combined cycle load decreases (Figs. 7(c) and 7(d)). However, here we have only analyzed these two extreme situations, and have not performed an optimization to investigate if there is an optimal load allocation that maximizes combined cycle efficiency. While this may be worthwhile to investigate, it is beyond the scope of this work.

The results shown in Fig. 6(a) confirm that sliding steam pressure control has a higher thermodynamic combined cycle efficiency compared to constant pressure operation, which is consistent with previous observations for steam bottoming cycles [22]. In Fig. 6(a), we also observe that the efficiency difference between sliding and constant pressure increases at low loads. When the load and exhaust heat from the gas turbines decreases, the steam turbine valve must reduce its opening, increasing throttling losses (Figs. 13(a) and 17(a)), to keep the steam pressure at the setpoint (Figs. 13(b) and 17(b)).

However, as seen in Figs. 12(b) and 16(b), the temperature response to sudden load changes is significantly improved when the pressure is controlled at a constant setpoint, especially for step changes. An interpretation of Fig. 8 can be that controlling the live steam temperature at the outlet of the OTSG contributes to keeping the temperature profile and phase regime inside the OTSG under a safe and operational region phase distribution, thus avoiding water droplets at the steam turbine inlet. During transients, keeping both temperature, with a model based non-linear transformation and feedback, and steam pressure controlled, can contribute to avoid entering into an unsafe OTSG operating mode where superheated steam is not being produced. This could happen with a relatively large feedwater mass flow rate in comparison to the gas turbine exhaust gas total enthalpy at the inlet of the OTSG.

Therefore, implementing pressure control might be required for rejecting unexpected setpoint changes for the combined cycle power load. In this work, this is exemplified as a trip in direct drive electrical motors in the offshore energy system, resulting in a sudden 15 MW_{el} combined cycle load reduction, as simulated at $t = 50$ min in Fig. 10. In practice, a compromise or a more advanced control structure that considers active constraint switches [52,57] may be implemented. For example, the load can be changed at a lower rate, as shown in Fig. 16(b), or logic can be used to activate the pressure controller when there are large load changes or sudden trips. For normal and continuous operation, one could recommend changing load setpoint using slow ramp changes, with the more efficient sliding pressure control structure for the bottoming cycle, which also results in lower specific CO_2 emissions.

Since the results in Table 4 suggest that emissions are not significantly affected by rate of change in load (ramp or step), one should prioritize steady-state operation when selecting a control structure, as long as disturbance rejection requirements are satisfied. Note that in some future offshore oil and gas energy system scenarios, such as systems integrating offshore wind, combined cycle power setpoint loads will probably be continuously changing. In that case, the transient conditions might be the normal operating condition, and the suitable control philosophy selection might depend on the typical trajectory and amplitude of the setpoint.

It also should be noted that despite the values in Table 4 would vary with different natural gas compositions or with a different set of setpoint changes, the trends and conclusions regarding efficiency and CO_2 emissions would remain the same. Moreover, if future offshore compact combined cycles are operated using carbon-free fuels such as hydrogen or ammonia instead of natural gas [2], the learnings from this contribution would still be highly relevant, as fuel efficiency would still be important.

5. Conclusions

In this work we analyze the operation and control problem for a *compact* combined cycle producing power on an offshore processing installation. The system is composed of two gas turbines and a bottoming steam cycle recovering waste heat in two compact OTSGs and converting it to power, thus increasing the thermodynamic efficiency and reducing the specific CO_2 emissions of the process. We present a steady-state performance evaluation of load allocation between the two gas turbines. We also present dynamic performance analysis of the combined cycle to power setpoint changes using different control approaches.

To allocate the load to the gas turbines, we compare two control structures. The first and more efficient approach implements feedforward such that the load is distributed equally and both gas turbines have the same setpoint (Fig. 3(a)). The second alternative implements one P-controller to use one gas turbine dynamically, but to keep it close to its nominal operation of 90% at steady-state, and one I-controller that manipulates the setpoint to the second gas turbine to satisfy the variable demand of power (Fig. 3(b)).

The main controlled variables for the bottoming cycle are the superheated steam temperature and pressure, with the main manipulated variables being the feedwater flowrate and steam turbine valve respectively. We implement systematically derived nonlinear model-based feedforward to control the temperature [22], and we compare sliding and constant pressure operation mode. Operating at sliding pressure increases the system's efficiency (Fig. 6(a)) because of a reduction in throttling losses, while operating at constant pressure (Fig. 12(b)) improves the temperature response to large and/or fast load changes. The outcome of this work can be used to analyze the operation and control of an integrated system with non-dispatchable renewable energy sources, where the compact combined cycle will be the only available manipulated variable for balancing demand and supply. Further, this work can be expanded to include the operation and control problem for offshore compact combined cycles producing both power and heat. Moreover, a more advanced upper control layer such as model predictive control may be implemented to optimally allocate the gas turbines loads, as well as the steam temperature and pressure setpoints subject to balancing demand and supply and satisfying the operational constraints.

CRediT authorship contribution statement

Rubén M. Montañés: Writing – review & editing, Writing – original draft, Validation, Methodology, Investigation, Formal analysis, Data curation. **Cristina Zotică:** Writing – original draft, Visualization, Software, Methodology, Investigation, Formal analysis, Data curation, Conceptualization. **Adriana Reyes-Lúa:** Writing – review & editing, Writing – original draft, Project administration, Investigation, Formal analysis, Conceptualization.

Declaration of competing interest

The authors declare that they have no known competing financial interests or personal relationships that could have appeared to influence the work reported in this paper.

Data availability

The data that has been used is confidential.

Acknowledgments

This publication has been produced with support from the LowEmission Research Centre (www.lowemission.no), performed under the Norwegian research program PETROSENTER. The authors acknowledge the industry partners in LowEmission for their contributions and the Research Council of Norway (296207). The authors acknowledge the contribution of our colleagues Geir Skaugen and Han Deng in developing the optimal design of the compact OTSGs. We acknowledge Siemens Energy, a partner in the LowEmission Research Centre, for providing the SGT-750 Modelica model used as reference.

References

[1] Norwegian Petroleum Directorate. Emissions to air. 2023, URL: https://www.norskpetroleum.no/en/environment-and-technology/emissions-to-air/.

[2] Voldsund M, Reyes-Lúa A, Fu C, Ditaranto M, Nekså P, Mazzetti M, et al. Low carbon power generation for offshore oil and gas production. Energy Convers Manage X 2023. http://dx.doi.org/10.1016/j.ecmx.2023.100347.

[3] Grainger D, Bindingsbø AU, Brekke O, De Koeijer G, Rekaa Nilssen O, Pettersen J. Reducing CO_2 emissions from offshore oil and gas production. In: Proceedings of the 15th greenhouse gas control technologies conference. SSRN; 2021, p. 12. http://dx.doi.org/10.2139/ssrn.3820726.

[4] Kloster P. Energy optimization on offshore installations with emphasis on offshore combined cycle plants. In: Offshore Europe oil and gas exhibition and conference. Society of Petroleum Engineers; 1999, http://dx.doi.org/10.2118/56964-MS, URL: www.onepetro.org/doi/10.2118/56964-MS.

[5] Oil & Gas UK. Offshore gas turbines and dry low NOx burners. 2015, URL: https://silo.tips/download/offshore-gas-turbines-and-dry-low-nox-burners-an-analysis-of-the-performance-imp.

[6] Nguyen T-V, Tock L, Breuhaus P, Maréchal F, Elmegaard B. Oil and gas platforms with steam bottoming cycles: System integration and thermoenvironomic evaluation. Appl Energy 2014;131:222–37. http://dx.doi.org/10.1016/j.apenergy.2014.06.034, URL: https://linkinghub.elsevier.com/retrieve/pii/S0306261914006163.

[7] Nord LO, Bolland O. Design and off-design simulations of combined cycles for offshore oil and gas installations. Appl Therm Eng 2013;54:85–91. http://dx.doi.org/10.1016/j.applthermaleng.2013.01.022.

[8] Gonzalez-Salazar MA, Kirsten T, Prchlik L. Review of the operational flexibility and emissions of gas- and coal-fired power plants in a future with growing renewables. Renew Sustain Energy Rev 2018;82:1497–513. http://dx.doi.org/10.1016/j.rser.2017.05.278.

[9] Bimüller JD, Nord LO. Process simulation and plant layout of a combined cycle gas turbine for offshore oil and gas installations. J Power Technol 2015;95:40–7.

[10] Montañés R, Skaugen G, Hagen B, Rohde D. Compact steam bottoming cycles: Minimum weight design optimization and transient response of once-through steam generators. Front Energy Res 2021. http://dx.doi.org/10.3389/fenrg.2021.687248.

[11] Montañés R, Hagen B, Deng H, Skaugen G, Morin N, Andersen M, et al. Design optimization of compact gas turbine and steam combined cycles for combined heat and power production in a fpso system – a case study. Energy 2023;282:128401. http://dx.doi.org/10.1016/j.energy.2023.128401.

[12] Mazzetti MJ, Hagen BA, Skaugen G, Lindqvist K, Lundberg S, Kristensen OA. Achieving 50% weight reduction of offshore steam bottoming cycles. Energy 2021;230:120634. http://dx.doi.org/10.1016/j.energy.2021.120634.

[13] Nord LO, Montañés RM. Compact steam bottoming cycles: Model validation with plant data and evaluation of control strategies for fast load changes. Appl Therm Eng 2018.

[14] ConocoPhillips. Utslippsrapport 2019 for eldfisk feltet (emissions report for the eldfisk field). 2019, URL: https://offshorenorge.no/contentassets/500573d7546748b888327ffd5e4ab519/eldfisk.pdf.

[15] Tulalian R, Keever E, Rastogi A. Shell appomattox model-based operations from design to production: A game changer in GoM deepwater operation. In: Offshore technology conference. 2020, http://dx.doi.org/10.4043/30838-MS.

[16] Equinor ASA. Final investment decision for bacalhau phase 1 in Brazil. 2021, URL: https://www.equinor.com/news/archive/20210601-final-investment-decision-bacalhau-phase1-brazil.

[17] Bowman T. Decarbonizing FPSO power plants: The case for combined cycle and electric-motor driven EMD compression. Houston, Texas, USA: OTC; 2022, D011S009R003. http://dx.doi.org/10.4043/32027-MS, URL: https://onepetro.org/OTCONF/proceedings/22OTC/1-22OTC/D011S009R003/484508.

[18] Zotică C, Alsop N, Skogestad S. Transformed manipulated variables for linearization, decoupling and perfect disturbance rejection. IFAC-PapersOnLine 2020. http://dx.doi.org/10.1016/j.ifacol.2020.12.2331.

[19] Deng H, Skaugen G, Næss E, Zhang M, Øiseth OA. A novel methodology for design optimization of heat recovery steam generators with flow-induced vibration analysis. Energy 2021.

[20] Skaugen G, Walnum HT, Hagen BAL, Clos DP, Mazzetti MJ, Nekså P. Design and optimization of waste heat recovery unit using carbon dioxide as cooling fluid. In: ASME 2014 power conference - POWER 2014 - vol. 1. American Society of Mechanical Engineers; 2014, http://dx.doi.org/10.1115/POWER2014-32165.

[21] Nord LO, Bolland O. Design and off-design simulations of combined cycles for offshore oil and gas installations. Appl Therm Eng 2013;54:85–91. http://dx.doi.org/10.1016/j.applthermaleng.2013.01.022, URL: https://linkinghub.elsevier.com/retrieve/pii/S1359431113000628.

[22] Zotică C, Montañés RM, Reyes-Lúa A, Skogestad S. Control of steam bottoming cycles using nonlinear input and output transformations for feedforward disturbance rejection. IFAC-PapersOnLine 2022;55:969–74. http://dx.doi.org/10.1016/j.ifacol.2022.07.570.

[23] Nord L, Bolland O. Steam bottoming cycles offshore - challenges and possibilities. J Power Technol 2012;92:201–7, URL: https://papers.itc.pw.edu.pl/index.php/JPT/article/view/346.

[24] Nord LO, Martelli E, Bolland O. Weight and power optimization of steam bottoming cycle for offshore oil and gas installations. Energy 2014. http://dx.doi.org/10.1016/j.energy.2014.08.090.

[25] Raddum A. Transient performance of siemens SGT-750 and SGT-800 : Modeling and simulations of industrial gas turbines on island grids [Master's thesis], Umeå University, Department of Applied Physics and Electronics; 2020.

[26] Siemens. SGT-750 gas turbines - technical data. 2023, URL: https://www.siemens-energy.com/global/en/home/products-services/product/sgt-750.html#/.

[27] Dassault Systèmes. DYMOLA systems engineering. In: Multi-engineering modeling and simulation based on modelica and FMI. 2019.

[28] Modelon AB. Thermal power library. 2020, URL: https://modelon.com/library/thermal-power-library/.

[29] LowEmission research center. 2019, URL: www.sintef.no/projectweb/lowemission/.

[30] Åberg M, Windahl J, Runvik H, Magnuson F. Optimization-friendly thermodynamic properties of water and steam. In: Proceedings of the 12th international modelica conference. 2017.
[31] McBride BJ, Zehe MJ, Gordon S. Nasa glenn coefficients for calculating thermodynamic properties of individual species. 2002, NASA/TP.
[32] Dechamps. Modelling the Transient Behaviour of Heat Recovery Steam Generators. Proc Inst Mech Eng A 1995.
[33] Cooke D. On prediction of off-design multistage turbine pressures by Stodola's ellipse. J Eng Gas Turbines Power 1985.
[34] Jonshagen K, Genrup M. Improved load control for a steam cycle combined heat and power plant. Energy 2010;35:1694–700. http://dx.doi.org/10.1016/j.energy.2009.12.019, demand Response Resources: the US and International Experience.
[35] Thulukkanam K. Heat exchanger design handbook. 2nd ed. CRC Press; 2013.
[36] Dumont M-N, Heyen G. Mathematical modelling and design of an advanced once-through heat recovery steam generator. Comput Chem Eng 2004;28:651–60. http://dx.doi.org/10.1016/j.compchemeng.2004.02.034, URL: https://www.sciencedirect.com/science/article/pii/S0098135404000341. eSCAPE 13.
[37] Hübel M, Meinke S, Andrén MT, Wedding C, Nocke J, Gierow C, et al. Modelling and simulation of a coal-fired power plant for start-up optimisation. Appl Energy 2017;208:319–31. http://dx.doi.org/10.1016/j.apenergy.2017.10.033, URL: https://www.sciencedirect.com/science/article/pii/S030626191731440X.
[38] Montañés RM, Gardarsdóttir S, Normann F, Johnsson F, Nord LO. Demonstrating load-change transient performance of a commercial-scale natural gas combined cycle power plant with post-combustion CO_2 capture. Int J Greenh Gas Control 2017;63:158–74. http://dx.doi.org/10.1016/j.ijggc.2017.05.011, URL: https://www.sciencedirect.com/science/article/pii/S1750583617300464.
[39] Martinez Castilla G, Montañés RM, Pallarès D, Johnsson F. Dynamics and control of large-scale fluidized bed plants for renewable heat and power generation. Appl Therm Eng 2023;219:119591. http://dx.doi.org/10.1016/j.applthermaleng.2022.119591, URL: https://www.sciencedirect.com/science/article/pii/S1359431122015216.
[40] Wang H, Hägglund T, Song Z. Quantitative analysis of influences of model plant mismatch on control loop behavior. Ind Eng Chem Res 2012;51:15997–6006. http://dx.doi.org/10.1021/ie300834y, URL: https://pubs.acs.org/doi/10.1021/ie300834y.
[41] Rivera DE, Morari M, Skogestad S. Internal model control: PID controller design. Ind Eng Chem Process Des Dev 1986;25:252–65. http://dx.doi.org/10.1021/i200032a041, URL: https://pubs.acs.org/doi/abs/10.1021/i200032a041.
[42] Åström KJ, Murray RM. Feedback systems: An introduction for scientists and engineers. Princeton: Princeton University Press; 2008, OCLC: ocn183179623.
[43] Skogestad S. Simple analytic rules for model reduction and PID controller tuning. J Process Control 2003. http://dx.doi.org/10.1016/S0959-1524(02)00062-8.
[44] Grimholt C, Skogestad S. Optimal PI-control and verification of the SIMC tuning rule. IFAC Proc Vol 2012;45:11–22. http://dx.doi.org/10.3182/20120328-3-IT-3014.00003, URL: https://linkinghub.elsevier.com/retrieve/pii/S1474667016309934.
[45] Zotică C, Nord LO, Kovács J, Skogestad S. Optimal operation and control of heat to power cycles: A new perspective from a systematic plantwide control approach. Comput Chem Eng 2020. http://dx.doi.org/10.1016/j.compchemeng.2020.106995.
[46] Skogestad S. Advanced control using decomposition and simple elements. Annu Rev Control 2023;56:100903. http://dx.doi.org/10.1016/j.arcontrol.2023.100903, URL: https://linkinghub.elsevier.com/retrieve/pii/S1367578823000676.
[47] Skogestad S, Zotică C, Alsop N. Transformed inputs for linearization, decoupling and feedforward control. J Process Control 2023;122:113–33. http://dx.doi.org/10.1016/j.jprocont.2022.12.012, URL: https://linkinghub.elsevier.com/retrieve/pii/S0959152422002414.
[48] Guzmán JL, Hägglund T. Tuning rules for feedforward control from measurable disturbances combined with PID control: a review. Internat J Control 2024;97:2–15. http://dx.doi.org/10.1080/00207179.2021.1978537, URL: https://www.tandfonline.com/doi/full/10.1080/00207179.2021.1978537.
[49] Hast M, Hägglund T. Low-order feedforward controllers: Optimal performance and practical considerations. J Process Control 2014;24:1462–71. http://dx.doi.org/10.1016/j.jprocont.2014.06.016, URL: https://linkinghub.elsevier.com/retrieve/pii/S0959152414001796.
[50] Zotică C, Skogestad S. Input transformation for linearization, decoupling and disturbance rejection with application to steam networks. In: Computer aided chemical engineering. Elsevier; 2021, http://dx.doi.org/10.1016/B978-0-323-88506-5.50157-1.
[51] Zotică Cristina. Optimal operation and control of thermal energy systems [Ph.D. thesis], Trondheim, Norway: Norwegian University of Science and Techology; 2023, URL: https://hdl.handle.net/11250/3054787.
[52] Reyes-Lúa A, Skogestad S. Systematic design of active constraint switching using classical advanced control structures. Ind Eng Chem Res 2020;59:2229–41. http://dx.doi.org/10.1021/acs.iecr.9b04511, URL: https://pubs.acs.org/doi/10.1021/acs.iecr.9b04511.
[53] Skogestad S. Near-optimal operation by self-optimizing control: from process control to marathon running and business systems. Comput Chem Eng 2004;29:127–37. http://dx.doi.org/10.1016/j.compchemeng.2004.07.011, URL: https://linkinghub.elsevier.com/retrieve/pii/S009813540400184X.
[54] Jäschke J, Cao Y, Kariwala V. Self-optimizing control – A survey. Annu Rev Control 2017;43:199–223. http://dx.doi.org/10.1016/j.arcontrol.2017.03.001, URL: https://linkinghub.elsevier.com/retrieve/pii/S1367578816301055.
[55] Qiu K, Andersson LE, Zotică C, Reyes-Lúa A, Montañés RM, Chabaud V, et al. Model predictive control of compact combined cycles in offshore power plants integrating a wind farm. Comput Aided Chem Eng 2023. http://dx.doi.org/10.1016/B978-0-443-15274-0.50246-8.
[56] Åström KJ, Hägglund T. Advanced PID control. ISA- International Society of Automation; 2006.
[57] Reyes-Lúa A. Systematic design of advanced control structures [Ph.D. thesis], Trondheim, Norway: Norwegian University of Science and Techology; 2020, URL: http://hdl.handle.net/11250/2646065.